ACS APPLIED MATERIALS & INTERFACES

www.acsami.org

Research Article

Mechanisms and Factors Influencing the Production of Uniform-Sized Giant Unilamellar Vesicles by Discrete Lipid Film Arrays

Yaqi Bai, Ning Hu,* Xinyu Duan, Jun Yang, and Huangxian Ju*

Cite This: *ACS Appl. Mater. Interfaces* 2024, 16, 45948−45955

Read Online

ACCESS | Metrics & More | Article Recommendations | Supporting Information

ABSTRACT: In this paper, we innovatively proposed a highly uniform vesicle preparation scheme based on the intervesicle mechanical self-constraint effect of vesicle crowding. By adjusting the spacing of discrete microwell structures, we observed that during the self-assembly of phospholipid molecules in microwells to form giant unilamellar vesicles (GUVs), the scale swelling of the vesicles during the continuous growth process would lead to the crowding of vesicles in adjacent microwells, thus inducing the formation of intervesicle mechanical self-constraint effect. The results of the experiment showed that this paper obtained the optimized discretized microwell structure (micropillar side: 30 μm; pitch: 0 μm), and the corresponding lipid mass was measured and determined, yielding homogeneous giant GUVs of 37.9 ± 2.0 μm. In this paper, homogenized GUVs (~40 μm) with different cholesterol concentrations (10, 20, and 30%) were obtained by this method, and the above vesicles were subjected to controlled electroporation experiment under external electric fields of 23, 31, and 41 kV/cm, respectively. It showed that the mechanical self-constraint effect of vesicle crowding induced by patterned microstructures during the self-assembly of phospholipid molecules significantly enhances the size homogeneity of GUVs, which would be helpful for the wide applications of GUVs in other areas such as cell-like models and controlled release of drugs.

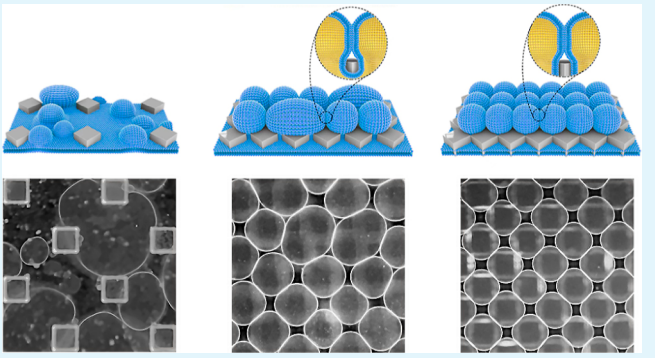

KEYWORDS: *giant unilamellar vesicles, size controlled, microwells, discrete lipid, mechanisms*

1. INTRODUCTION

Giant unilamellar vesicles (GUVs) are composed of phospholipid materials with sizes ranging from 5 to 200 μm.[1] Phospholipids can spontaneously form closed structures with internal environments through the formation of phospholipid bilayer membranes.[2] They are widely used in research as cell-like model systems,[3−5] vesicle fusion,[6] microscale reactors,[7] and so on due to their similarity in size and curvature to cells. The traditional hydration method of dried lipid films is commonly used to form vesicles. It includes the gentle hydration method[8,9] and electroformation method.[10−12] These methods are always difficult to control the vesicle size with the coefficients of variation of 61.5 and 52.8%, respectively.[13] Therefore, effective control of the size of GUVs becomes a key challenge, especially when their size has a significant influence on the application performance. For example, in drug therapy, the size of GUVs determines the dosage and targeting efficiency,[14] while the transmembrane voltage in vesicle electroporation is closely related to the size of the vesicles.[15] Notably, despite the challenging size control of vesicles, studies have proposed simple methods to reduce the size distribution of GUVs, e.g., Tamba et al. proposed a new membrane filtration method for purifying and separating GUVs of uniform size (10−30 μm).[16] Furthermore, size control also affects the interactions between the lipid membrane and encapsulated molecule,[14,17] molecular transport across biological membranes,[18,19] and membrane mechanical properties.[20,21] Therefore, the preparation of controllable-sized GUVs has gained considerable attention in recent years.

Currently, two main types of vesicle preparation methods have been proposed to solve the problem of particle size control. One is the microfluidic method,[22] and the other is based on microfabrication techniques.[23−27] The microfluidic method can solve the problem of vesicle preparation in high salt solution and can also effectively control the particle size of GUVs, that is, there is the residue of organic solvent. The residue of organic solvent changes the physicochemical properties of GUVs, thus affecting subsequent research. Therefore, although this method has been developed, the traditional hydration method is still used for the formation of vesicles.

Received: May 14, 2024
Revised: August 14, 2024
Accepted: August 14, 2024
Published: August 21, 2024

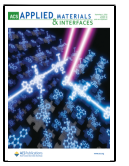

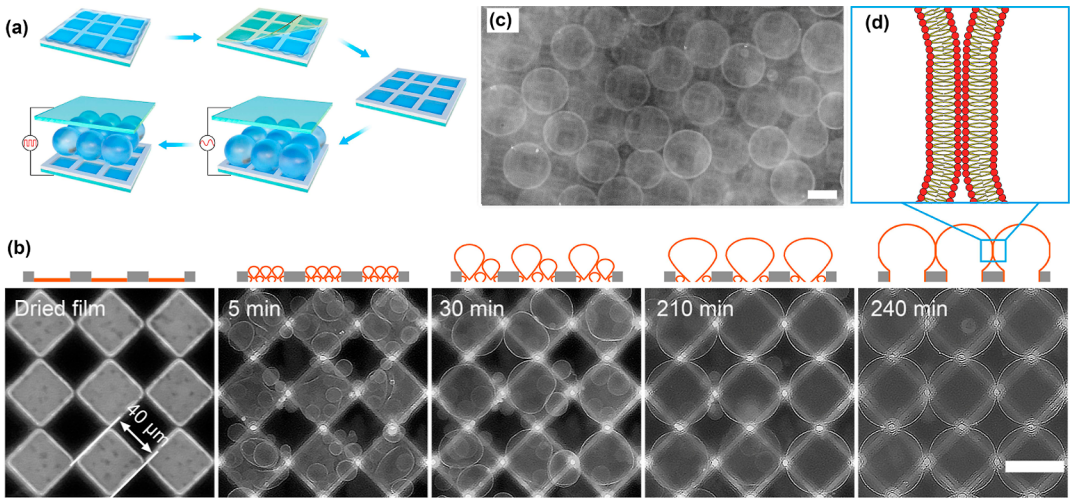

Figure 1. Vesicle formation within the microwell array. (a) Schematic illustration of the whole process of vesicle formation. (b) Process of vesicle growth from the microwells. (c) Detached vesicles after applying a signal of square wave to top and bottom ITO electrodes. (d) Membrane structure at an interface of two neighboring vesicles. Scale bar: 50 μm.

It has been demonstrated that the size and thickness of the initial lipid film deposits directly affect the size distribution of vesicles.[4] Therefore, various microfabrication techniques have been developed, such as microcontact printing[23,24] and micropillar film-forming method.[25−27] Selective deposition of dried phospholipid films results in the formation of discrete membrane arrays. GUVs of uniform size are formed by hydrating discrete lipid film arrays. Both methods are more effective, but the shedding of GUVs is still problematic. In addition, its mechanism is not yet clear. Here, it is worth noting that it must be a discrete film. Le Berre et al. deposited dried phospholipid films on silicon wafers containing microcolumn and micropillar arrays, respectively; however, they did not remove the excess lipids outside the microstructure.[28]

In a previous study, vesicles swell to form liposome precursors.[29] These liposome precursors continue to fuse over the next time; this process is referred to as vesicle fusion. It was hypothesized that excessive vesicle fusion may be a significant factor contributing to the inhomogeneous size of GUVs. The deposition of discrete dry lipid films using microwell and micropillar film-forming methods could prevent fusion between discrete films and thus control the particle size of GUVs. To verify this idea, this study used microwell arrays with different spacings to physically confine vesicle fusion to varying degrees as a means of investigating the effect of vesicle fusion on the formation of GUVs (Figure 1a). It could be concluded that vesicle fusion was the main pathway for membrane swelling and uncontrolled vesicle fusion was indeed a key factor leading to the inhomogeneous particle size of GUVs. Uniform deposition of dried lipid films into closed microwells effectively controlled vesicle fusion to occur only within the microwells. By adjusting the spacing of discrete microwell structures during the self-assembly of phospholipid molecules, we observed that the gradual swelling of the vesicles throughout the growth process resulted in vesicle crowding within neighboring microwells. This phenomenon induced the emergence of an intervesicle mechanical self-constraint effect, which led to highly homogeneous GUVs. The factors affecting the formation of uniform GUVs from discrete film arrays and the effect of cholesterol concentration on GUV electroporation were also explored. By effectively controlling these factors, researchers can obtain their ideal-sized GUVs for subsequent application studies, thus eliminating the tedious purification process.

2. RESULTS AND DISCUSSION

2.1. Vesicle Formation. As shown in Figure 1a, in this study, chips with microarray structures (microwells) were fabricated by photolithography, and lipid films were deposited on the microchips. After the formation of the dry film, the lipids outside the microwells were removed using the PET film to take advantage of the microstructural height difference, leaving only the lipids inside the microwells (Figure S1). To increase the high uniformity of the lipid film, a multidroplet technique of lipid film formation was used (Figure S2).

In the vesicle formation process, vesicle fusion or bud merging is the predominant pathway for vesicle growth (Figure 1b). Subsequently, dome-shaped vesicles filled the microwells, and when a square-wave signal was applied to the indium tin oxide (ITO) electrodes for about 1 h, the dome-shaped vesicles detached from the bottom ITO electrode to form enclosed GUVs (Figure 1c). During vesicle formation, the small vesicles gradually fused into a large vesicle, and eventually there was only one vesicle per microwell (Figures 1b and S3). The fusion phenomenon was thought to only occur in vesicle electroformation and was induced by an electric field;[10] however, it was also observed in vesicle formation by gentle hydration in our previous studies,[29] as well as by gel-assisted swelling in many other studies.[11,30−32] Therefore, vesicle fusion was the predominant pathway for vesicle growth in hydration methods and not just electroformation.

In the first 30 min, vesicle growth was rapid, so there were some differences in vesicle sizes, but due to the similar mass of lipids in each micropore and the consistent growth environment, this reduced the intervesicle differences to some extent. As the vesicles enlarged, the internal pressure and surface tension were balanced, the vesicle growth slowed down, and the differences between microwells were reduced. At 210 min, spatial constraints and repulsive effects led to a convergence of the vesicle sizes in each microwell. At 240 min, vesicle contact was intensified and the growth rate gradually converged under

https://doi.org/10.1021/acsami.4c07934
ACS Appl. Mater. Interfaces 2024, 16, 45948−45955

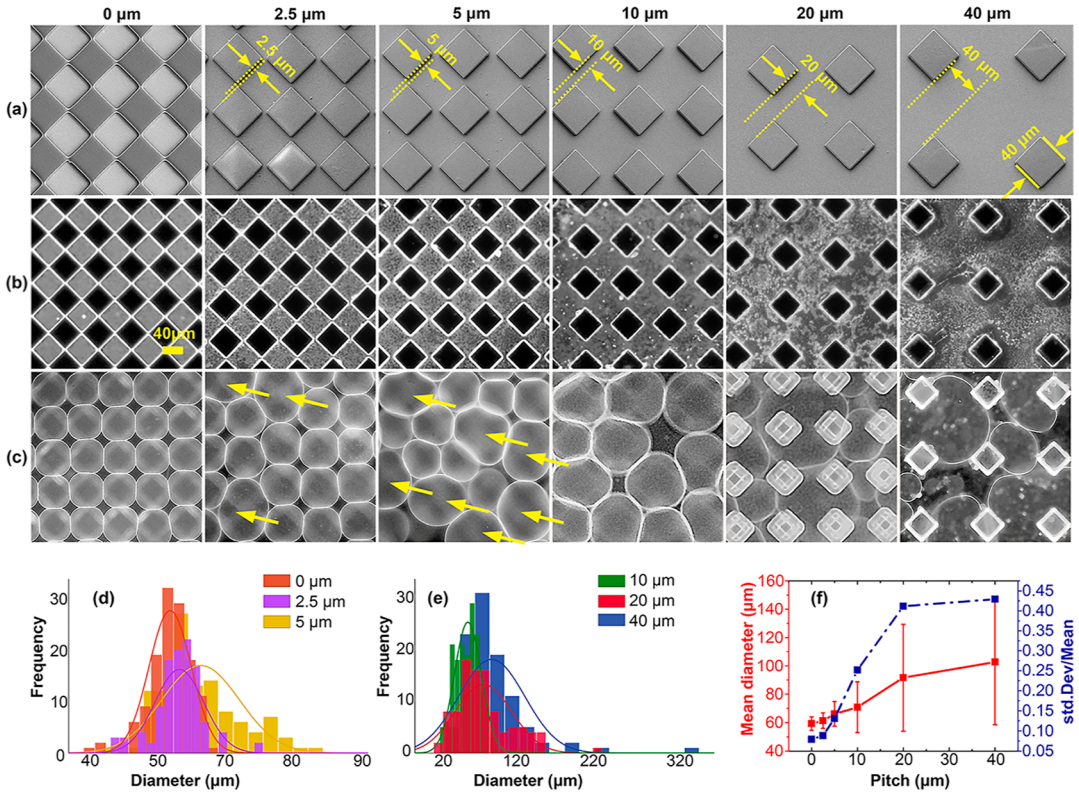

Figure 2. Effect of film continuity on vesicle fusion. (a) SEM images of the micropillar arrays with varying pitch. The pitch sizes (0, 2.5, 5, 10, 20, and 40 μm) were set following the size of the micropillar [Figure S6(b1)]. (b) Corresponding results of lipid deposition and (c) formed vesicles on these surfaces. (d–f) Size distribution and average diameters of the generated vesicles with respect to the pitch sizes (for each spacing condition, the sample size N = 130 is derived from sampling across 3 independent experiments). Scale bar: 40 μm.

the combined effects of mutual constraints and spatial site resistance.

Each microwell and vesicles growing from neighboring microwells were squeezed with each other but did not fuse (Figures 1b and S3). It was probably because the microwells isolated lipid films from outside. Vesicles growing from the isolated films had ordered outer layers (monolayers or bilayers) at the lipid–water interfaces (Figure 1d). Fusion among these vesicles did not occur until the ordered outer layers were ruptured and also did not occur in vesicle formation with the absence of fusogenic substances (such as many multivalent cations)[33,34] or external driving force (such as an electric field).[35]

2.2. Effect of Film Continuity on Vesicle Fusion. To verify and further investigate the effect of the discreteness of lipid films on vesicle fusion, a series of micropillars (5 μm in height) were fabricated on the ITO glass in a square array with a varying pitch size (Figure 2a). The connection of the micropillars formed closed microwells. Separation of the micropillars laterally opened the microwells and made them connect with each other. After lipid deposition, films with different degrees of continuity were formed on these structures (Figure 2b). The thickness uniformity of the films was found to decrease as the separation of micropillars increased, since leaving the organic solution to evaporate in a small space may mitigate the coffee ring effect (CRE).

Figure 2c shows the corresponding results of vesicle formation on these structures. The closed microwell group had the best results in terms of vesicle size uniformity. Fusion only occurred within each microwell, and vesicles growing from different microwells did not coalesce. The final vesicles after 4 h had the smallest average diameter of 59.3 μm ± 4.9 μm (micropillar side was 40 μm) and the narrowest size distribution of p = 0.08, where p = std. Dev/Mean, and std. Dev and Mean were the standard deviation and average diameters of the vesicles, respectively. Previous studies have suggested that vesicle detachment during electroforming often necessitates aids like electricity or ultrasonication.[24,36] The addition of a low-frequency square wave signal (4 Hz, 2 Vpp) caused the GUVs to detach from the substrate (Figure 1c and Movie S1), and the size distribution of the vesicles was 55.9 ± 4.9 μm (Figure S4). The morphology and size of the GUVs may be fine-tuned by the surface tension and hydrodynamics during detachment from the microwell substrate, and the vesicles may have an ellipsoidal shape when they are on the substrate due to the presence of hydrostatic pressure. However, the experimental data showed that the size changes of GUVs before and after detachment were slight and the vesicle size distribution remained consistent, indicating that the detachment process had a limited effect on the size characteristics of GUVs.

As the microwells laterally opened and the openings widened, vesicles fused with their neighboring-growing ones (as indicated by the arrows in Figure 2c) and the number of these coalesced vesicles increased as the openings widened, resulting in the formation of vesicles with a larger average size and wider size distribution (Figure 2d–f). It is worth noting that the error bars reflect the homogeneity of the vesicles, i.e., the larger the error bars, the more inhomogeneous the vesicles are. Apart from 40 μm of micropillars, the other two different sizes (30 and 50 μm) were also investigated whose results are shown in Figure S5. Therefore, it can be concluded that vesicle

https://doi.org/10.1021/acsami.4c07934
ACS Appl. Mater. Interfaces 2024, 16, 45948–45955

fusion is the predominant pathway for vesicle growth when hydration methods are employed, and uncontrollable vesicle fusion is responsible for the wide size distribution of vesicles.

Utilization of discrete lipid film arrays that are usually deposited in microwells to confine vesicle fusion within the isolated films of uniform size results in the formation of uniform vesicles. This mechanism can also explain why depositing lipids on nanocellulose paper with surfaces composed of entangled cylindrical nanofibers improved vesicle yield.[32] Schroder et al. demonstrated that no bilayer fusion but bud merging occurred in vesicle formation by observing if there was a "fusion event" between growing vesicles marked with red fluorescent labels and vesicles that had been prepared previously marked with green fluorescent labels.[11]

With regards to the driving force for vesicle fusion, it was thought to originate from vesicle crowding.[37] In this study, the depth of the microwells was ~5 μm, while the generated vesicles had diameters of several tens of micrometers. In other words, the microwells were too shallow to affect the crowding among the vesicles that grew from the neighboring microwells. However, fusion among these neighboring-growing vesicles was extremely low (less than 1%). Therefore, vesicle fusion was not driven by vesicle crowding. Figure 3 provides an alternative explanation that vesicle fusion may be induced by the penetrated water clusters that have not been fully enclosed by the lipid heads.

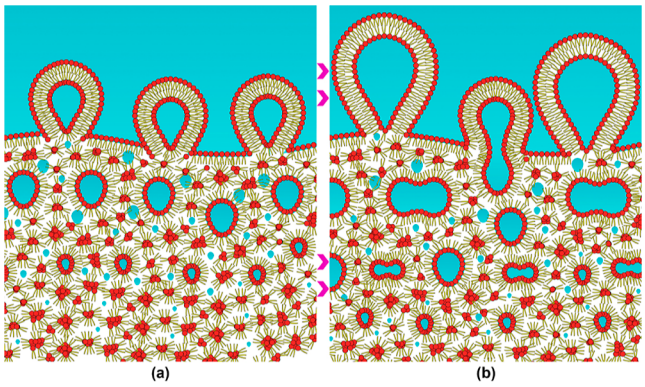

Figure 3. Schematic illustration of the vesicle fusion. (a) Formation of monolayer vesicles within lipid membranes. (b) Vesicle fusion.

Specifically, based on the SEM image of dried lipid films captured in our previous studies (Figure S7), lipids should be deposited on a solid substrate not in the form of bilayers as many studies believed,[32,38] because there is no macroscale hydrophilic surface similar to that provided by water, but in the formation of chain-like clusters with lipid heads to heads because interactions among polar lipid heads are stronger than those among nonpolar lipid tails. After water was added to the dried film, it penetrated the lipid film through the cracks among the lipid clusters. The penetration of water led to film swelling and the penetrated water clusters forced their surrounding lipid molecules to rearrange under hydrophobic effect, resulting in separation of the lipid phase and the water phase and the formation of monolayer vesicles within the lipid film (Figure 3a). This corresponds to the results of the first 15 min of the experiment in Figure S3, where multiple vesicles were dispersed in the microtiter wells, and since water penetration was gradually shielded by lipids, big vesicles were distributed on top and small ones were distributed on the bottom. The remaining water clusters that were not enclosed by polar lipid heads continued to force their surrounding lipid molecules to rearrange, thus mediating vesicle fusion (Figure 3b), and corresponding to the experimental results of the 20th−80th min in Figure S3, the small vesicles fused within the microwells to become larger and form larger single vesicles. After all of the penetrated water clusters were enclosed by lipid heads, vesicle fusion stopped, as shown after 160 min in Figure S3.

It is worth noting that despite the differences between cell electroformation and hydration law in the specific mechanisms triggering vesicle fusion (driving force and vesicle characteristics), both show similarities in the process of vesicle enlargement, i.e., when two small vesicles are in close proximity, their membranes may locally fuse to form a larger vesicle.

2.3. Compression among Vesicles. To determine the impact factors of this method, more experiments were carried out. Crowding among the vesicles growing from neighboring microwells did not cause fusion; instead, it changed the swelling barycenter of vesicles [Figure 4a(i,ii)] and confined the horizontal swelling of vesicles [Figure 4a(iii)]. In addition, fluorescence confocal microscopy was used to vertically scan the dome-shaped vesicles with a scanning step length of 1 μm, which showed almost the same height as long as enough lipids were deposited in the microwells (Movie S2). This was because these vesicles had almost the same supporting width (i.e., the microwell width), which determined the maximum swelling height of vesicles because of surface tension or hydrostatic pressure. Therefore, by taking advantage of these confinements produced by the horizontal crowding and vertical swelling limitation, the monodispersity of the vesicle might be improved. Thus, a series of concave microwell arrays varying in pitch size on the chip were fabricated [Figure 4b(i)]. The formed lipid film arrays within these microwells had different distributions of discreteness. The wide distribution of lipid films allowed vesicles to swell freely, while the close distribution of lipid films led to vesicle crowding [Figure 4b(ii)]. The vesicle crowding combined with the limitation of swelling height led to the formation of vesicles with narrow size distribution [Figure 4b(iii)] and small diameter [Figure 4b(iv)].

2.4. Electroporation of Vesicles in Different Membrane Compositions. Lipid concentration of the organic solution also remarkably affected vesicle formation. At low lipid concentrations, there were multiple small vesicles within the microwells that did not fuse into large vesicles. This may be due to the relative insufficiency of the total amount of phospholipids during the experiment, resulting in limited raw materials for vesicle formation within the microwells, or due to the more dispersed distribution of the lipid layer at the bottom, which fails to form a compact structure conducive to vesicle fusion.

Figure S8a illustrates the results of the preparation at low concentrations of phospholipid solution when vesicles were grown for 240 min. These discrete films formed vesicles that did not fuse. This phenomenon happened when the lipid concentration was lower than 0.12 mg/mL for 30 μm microwells. The thresholds were 0.15 and 0.18 mg/mL for 40 and 50 μm microwells, respectively. Six microliters of lipid solutions were used in all experiments. By comparison, a moderate lipid concentration led to the formation of only one vesicle in each microwell. These vesicles had similar sizes and

https://doi.org/10.1021/acsami.4c07934
ACS Appl. Mater. Interfaces 2024, 16, 45948−45955

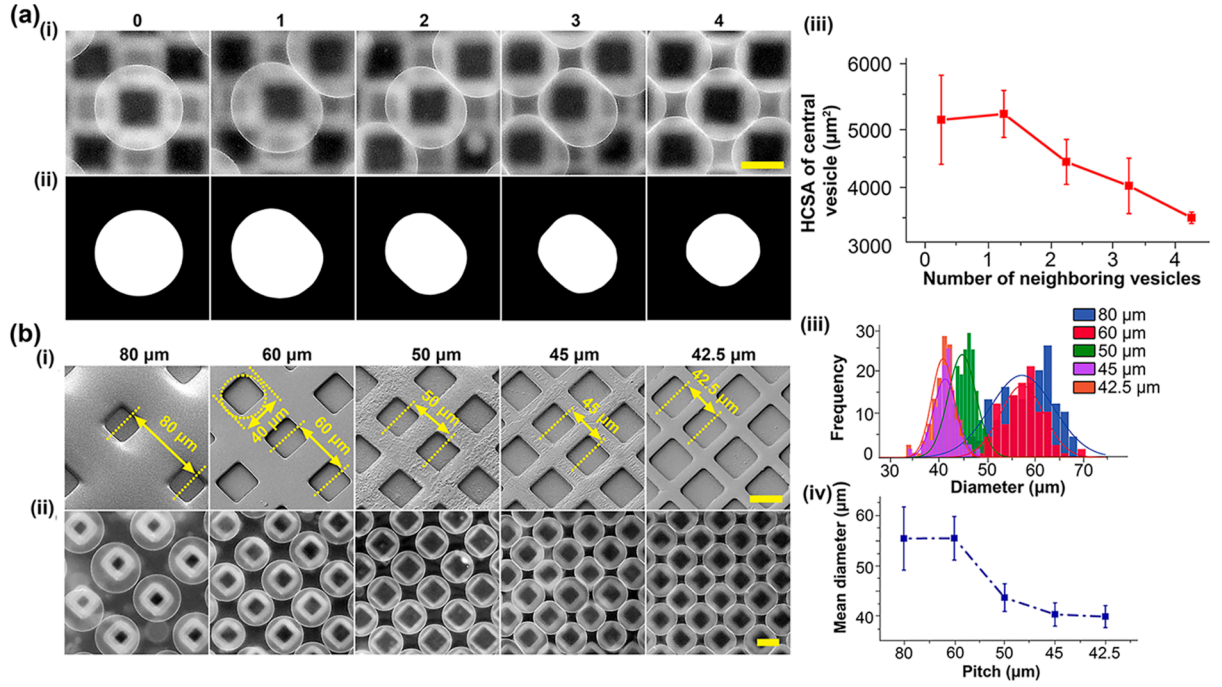

Figure 4. Effects of the compression among vesicles on vesicle formation. (a) Vesicle squeezing: (i) change of the swelling pattern of the vesicles upon squeezing by different vesicles; (ii) corresponding outlines of vesicles; and (iii) correlation between the horizontal cross-section area of the central vesicles shown in (i) and number of neighboring vesicles (number of experiments n = 5). (b) Vesicle preparation in different pitches of microwells: (i) SEM topography of the microwell arrays varying in pitch and (ii) corresponding results of vesicle formation within these microwells, the pitch sizes (80, 60, 50, 45, and 42.5 μm) were set based on the microwell size [Figure S6(b2)]. (iii,iv) Size distributions and mean diameters of the generated GUVs (for each spacing condition, the sample size N = 130 is derived from sampling across 3 independent experiments). Scale bar: 30 μm.

benefited from the confinements produced by the horizontal crowding and vertical swelling limitation. The generated vesicles decreased in average sizes with a decrease in the microwell diameter. However, a large lipid concentration led to the formation of multiple vesicles in each microwell which did not fuse (Figure S8c). This could be attributed to the formation of thick films in the microwells. Lipids on the surface of the thick film were unstable due to the absence of adhesion with the deposition substrate.[28] These unstable lipids were easily detached by osmotic force produced by water penetration, assembling into vesicles isolated from the bulk film. These isolated vesicles, on the one hand, did not coalesce because of having ordered membrane structures and, on the other hand, inhibited water penetration, causing inadequate swelling of the bottom lipids, and finally resulting in no formation of GUVs with good quality. The moderate ranges of lipid concentration were 0.12−0.2 mg/mL for 30 μm microwells, 0.15−0.25 mg/mL for 40 μm microwells, and 0.18−0.29 mg/mL for 50 μm microwells. The vesicle formation under these conditions is shown in Figure S9.

Combined with the rigorous fitting of the standard curve (Figure S10), we successfully implemented quantitative lipid analysis in microwells, and we were able to stably prepare vesicles with a high degree of homogeneity in 30 μm microwells when the lipid mass reached $2.7 \times 10^7 \pm 4.6 \times 10^9$ mg. Similarly, in 40 and 50 μm microwells, the required lipid masses were $4.7 \times 10^7 \pm 8.7 \times 10^9$ and $7.4 \times 10^7 \pm 1.5 \times 10^9$ mg (Table S1), respectively, and these conditions likewise supported the efficient generation of homogeneous vesicles.

In this experiment, GUVs with diameters of approximately 40 μm were prepared. Their cholesterol concentration was regulated, finding that homogeneity of vesicles could be achieved under our experimental system in all cases (Figure 5a). Based on this experimental result, we further introduced green 5-carboxyfluorescein (CF) to label the interior part of the GUVs (Figure 5b), which facilitated the subsequent observation of the fluorescence leakage phenomenon caused by electroporation by fluorescence microscopy. After centrifugation to remove the excess fluorescent dye from the periphery of GUVs, the vesicle suspension was placed in a special electrode device (Figure 5c). High voltage pulses (amplitude: 200−500 V, pulse width: 100 μs, pulse interval: 1 s, number of pulses: 100) were applied by using a cell fusion instrument.

Due to the difficulty in directly measuring the transmembrane voltage, the minimum applied electric field intensity required for electroporation in GUVs was defined in this study as the applied threshold electric field for electroporation (Figure 5d). A positive correlation between the vesicle electroporation threshold and the cholesterol concentration was observed. Further analysis showed significant differences in the proportion of GUVs undergoing electroporation for different cholesterol concentrations (10, 20, and 30%) at electric field strengths ranging from 20 to 50 kV/cm (Figure 5e). In particular, the proportion of GUVs with high cholesterol concentrations undergoing electroporation was significantly lower at the same electric field strength; e.g., only a few GUVs with 30% cholesterol concentration underwent electroporation at an electric field of 30 kV/cm (13.3% ± 4.1%), which was much lower than that at low cholesterol concentrations, where the proportion of electroporation was as high as 90.0% ± 4.0% for GUVs with 10%

https://doi.org/10.1021/acsami.4c07934
ACS Appl. Mater. Interfaces 2024, 16, 45948−45955

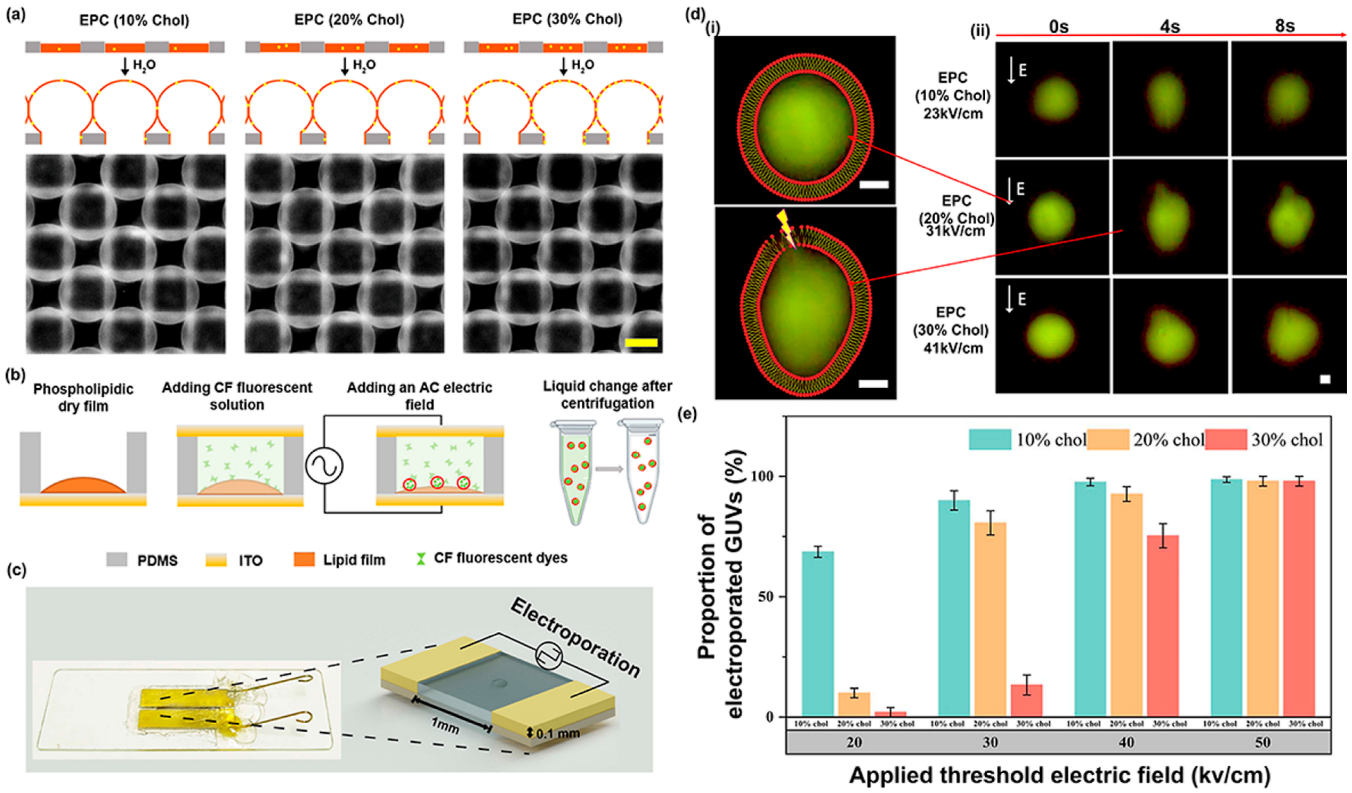

Figure 5. (a) Effects of lipid concentration on vesicle formation and the corresponding schematic diagrams. The microwell width was 50 μm. Scale bar: 40 μm. (b) Experimental procedure for the preparation of internally fluorescent GUVs. (c) Electrode unit. (d) (i) Schematic diagram of vesicles in the state of unelectroporation and critical electroporation and (ii) processes of the vesicles from unelectroporation to critical electroporation. Scale bar: 10 μm. (e) Percentage of perforation of GUVs with different cholesterol concentrations at different electric field intensities. Each column represents the average of five replicates (N = 5) and the number of samples is 50 at a time.

cholesterol concentration and 80.7% ± 5.0% for GUVs with 20% cholesterol concentration.

This finding suggests that effective control of the electroporation process can be achieved by modulating the cholesterol content in GUVs. Selective electroporation of different types of liposomes and the release of substances from the liposomes can be achieved using external electric fields and other modulations. This approach allows for the creation of microenvironments that can be controlled independently, providing a platform for investigating the biological mechanisms of organisms like cells. This technology platform not only contributes to an in-depth understanding of the electroporation mechanism of biofilms but also provides an important tool for research in the fields of gene transfection, drug delivery, and antitumor drug development.

3. CONCLUSIONS

In this study, a technique utilizing discrete film arrays to effectively regulate vesicle size and homogeneity was developed for the first time based on the mechanical self-constraint effect of crowding vesicles. Experimental results show that vesicle enlargement predominantly occurred through coalescence within each microwell, which was constrained by the presence of discrete lipid films. These films, upon hydration, form highly ordered outer layers that inhibit the coalescence of vesicles from adjacent microwells due to hydration-induced repulsion, resulting in the formation of vesicles of specific sizes. More importantly, during vesicle self-assembly, the spacing of discrete microstructures was adjusted to cause adjacent vesicles to come into proximity when the vesicles swelled and became larger, thus inducing the self-constraint effect between vesicles and controlling the disordered self-assembly of vesicles. The collected vesicles had a high degree of homogeneity of 37.9 ± 2.0 μm, and controlled electroporation occurred by the obtained homogeneous GUVs with different cholesterol concentrations and applying different voltages, respectively. The validated method paves the way to controllably produce monodisperse GUVs, which may reduce the necessity for time-consuming selection processes in future applications.

4. EXPERIMENTAL SECTION

4.1. Materials and Devices. Lipid L-α-phosphatidylcholine (egg, chicken, 99%) was purchased from Avanti (Alabaster, AL, USA). Fluorescent dye (DiI,1,1′-dihexadecyl-3,3,3′,3′-tetramethylindocarbocyanideperchlorate, ex/em: 549:564 nm, Molecular Probes, 98%) was purchased from Sigma-Aldrich (St. Louis, USA). Chloroform (99%) was purchased from Ke Long Chemical Co. (Chengdu, China). ITO was purchased from Kaivo (Shenzhen, China). Polydimethylsiloxane (PDMS) and curing agent were purchased from Dow Corning (Midland, USA). SU-8 3005 and its developer were purchased from MicroChem (MA, USA). IX73 fluorescence microscope (Olympus, Japan) and Leica SP8 confocal fluorescence microscope (Leica, Germany) were used for experimental observation. BEX LF301 cell fusion instrument was purchased from BEX (Tokyo, Japan).

4.2. Chip Fabrication. The chip consisted of four parts, as shown in Figure S6a: a top ITO electrode, a PDMS container (~3 mm in thickness), a layer of microstructures (arrays of microwells and micropillars) made of SU-8, and a bottom ITO electrode. The layer of microstructures was fabricated on the bottom ITO electrode with the standard lithography technology. Two types of microstructures were adopted in this study: concave microwells and convex micropillars (Figure S6b). The microwells and the micropillars had 5 and 6

https://doi.org/10.1021/acsami.4c07934
ACS Appl. Mater. Interfaces 2024, 16, 45948−45955

pitches, respectively, labeled as "d" in Figure S6b, and had a depth and height of 5 μm. Meanwhile, each of the microwells was a square with a length of D = 28.3 μm, while horizontal cross-section of each micropillar was also a square, and three different sizes of the micropillars D = 30, 40, and 50 μm were considered. Therefore, 23 kinds of microstructure patterns in total were designed in this study, whose physical pictures are shown in Figure S6c,d. To reduce the negative impacts of experimental operation and environmental conditions, all these microstructure patterns were arranged on the same ITO glass. As shown in Figure 5e, each pattern occupied an area of 7 × 7 mm.

For the chip fabrication, an ITO glass was spin-coated with an SU-8 film at 3000 rpm, resulting in a thickness of ∼5 μm. Then, the SU-8-coated ITO glass was carried out with a series of typical operations of soft photolithography, including soft-baking at 95 °C for 2 min, UV-light exposure for 30 s, postbaking at 65 °C for 1 min and 95 °C for 5 min, development at room temperature for 30 s, and hard baking at 150 °C for 30 min, to obtain an ITO glass with arrays of SU-8 microstructures. Finally, the microstructure-coated ITO was treated with oxygen plasma at 150 °C for 120 s. After lipid deposition on the microstructure-coated ITO (the details will be discussed in Section 2.3), it was assembled with the PDMS container and the top electrode, forming a complete chip for vesicle formation as shown in Figure S6a.

4.3. Lipid Film Formation. To prepare lipid solutions with specific concentrations, a certain amount of PC was dissolved in chloroform, followed by addition of fluorescent dye (DiI in dimethyl sulfoxide) with a mass ratio of lipid and DiI at 99.5:0.5. Then, 6 μL of lipid solution was loaded on the surface of the 7 mm × 7 mm microstructure-coated ITO glass. To increase the height uniformity of the lipid film, a multidroplet technique of lipid film formation was used, which leveraged the CRE.[39] Specifically, 6 μL of lipid solution was loaded serially in four steps: 1, 1.4, 1.6, and 2 μL, on the same spot of our device, forming progressively larger droplets on the spot. Figure S1 shows the remarkable improvement of film uniformity by using this new lipid film formation technique after the entire process of film formation.

After serial loading of the lipid solution, the glass was placed under vacuum (0.1 MPa) for 1 h to completely remove solvent (chloroform). To remove the lipids that were deposited outside the microwells, a PET film was used to cover the lipid-coated glass and then peel it off. This operation was repeated several times to ensure that almost all lipids that were distributed outside of the microwells were removed. Finally, the bottom ITO glass with patterned lipid films was assembled with a PDMS container and the top electrode, forming the complete chip for vesicle growth as shown in Figure S6a.

4.4. Vesicle Electroformation. After the chip was assembled, an AC signal (10 Hz, 2 Vpp) was applied to the ITO electrodes for several hours (usually 2 h) followed by the addition of 1.5 mL of deionized water into the chamber from the gap between the PDMS and top electrode. After the lipid film swelled completely and good vesicles were formed, a square-wave signal (4 Hz, 2 Vpp) was applied for another 1 h to detach the vesicles from the bottom ITO glass. The whole process was observed under an Olympus IX 73 fluorescence microscope. A Leica SP8 confocal fluorescence microscope was also used to observe the results when necessary.

4.5. Lipid Mass Measurement. Images showing different lipid masses, ranging from 2×10^{-4} to 2×10^{-3} mg in steps of 2×10^{-4} mg (a total of ten sets of concentrations in a single experiment, repeated three times), were observed under a fluorescence microscope, and the relevant fluorescence intensities were obtained by software processing, subtracted from those of the blank group, and linearly fitted to obtain a standard curve: $y = 1.63 \times 10^{8} + 8.24 \times 10^{11}x$ where $R^2 = 0.996$. In this step, we ensured that the fluorescence microscope settings (e.g., light source intensity, exposure time, gain, etc.) were consistent from one shot to the next to minimize errors caused by different settings.

In three independent experiments, the fluorescence intensity of the structures with their surfaces erased by the PET film was measured and calculated, yielding the fluorescence intensity of individual microwells (to avoid errors, the fluorescence intensity of a large area was counted here, and the fluorescence intensity of individual microwells was obtained by dividing the overall fluorescence intensity by the number of microwells).

■ ASSOCIATED CONTENT

Supporting Information

The Supporting Information is available free of charge at https://pubs.acs.org/doi/10.1021/acsami.4c07934.

Film removal; film formed; process of vesicle growth; size distribution of GUVs before and after detachment from microwells; vesicle formation on the surface patterned with micropillar arrays of different sizes; details of the microchip; SEM images of lipid deposition on an ITO glass; effect of lipid concentration on vesicle preparation; preparation of vesicles of different sizes; fitted curves for lipid mass and fluorescence intensity; and lipid mass at three structural scales (PDF)

Process of vesicle detachment from the base (MP4)

Confocal microscopy vertical scanning of dome-shaped vesicles (MP4)

■ AUTHOR INFORMATION

Corresponding Authors

Ning Hu − *Key Laboratory of Biorheological Science and Technology (Chongqing University), Ministry of Education, Bioengineering College, Chongqing University, Chongqing 400030, China;* orcid.org/0000-0002-6902-3302; Email: huning@cqu.edu.cn

Huangxian Ju − *State Key Laboratory of Analytical Chemistry for Life Science, School of Chemistry and Chemical Engineering, Nanjing University, Nanjing 210023, P. R. China;* orcid.org/0000-0002-6741-5302; Email: hxju@nju.edu.cn

Authors

Yaqi Bai − *Key Laboratory of Biorheological Science and Technology (Chongqing University), Ministry of Education, Bioengineering College, Chongqing University, Chongqing 400030, China*

Xinyu Duan − *Key Laboratory of Biorheological Science and Technology (Chongqing University), Ministry of Education, Bioengineering College, Chongqing University, Chongqing 400030, China*

Jun Yang − *Key Laboratory of Biorheological Science and Technology (Chongqing University), Ministry of Education, Bioengineering College, Chongqing University, Chongqing 400030, China;* orcid.org/0000-0001-6877-8677

Complete contact information is available at: https://pubs.acs.org/10.1021/acsami.4c07934

Author Contributions

The manuscript was written through contributions of all authors. All authors have given approval to the final version of the manuscript.

Notes

The authors declare no competing financial interest.

■ ACKNOWLEDGMENTS

This research was supported by the National Natural Science Foundation of China (32071408, 21827812, and 81871450).

REFERENCES

(1) Karamdad, K.; Law, R. V.; Seddon, J. M.; Brooks, N. J.; Ces, O. Preparation and Mechanical Characterisation of Giant Unilamellar Vesicles by a Microfluidic Method. *Lab Chip* **2015**, *15*, 557−562.

(2) Suharyani, I.; Mohammed, A. F. A.; Muchtaridi, M.; Wathoni, N.; Abdassah, M. Evolution of Drug Delivery Systems for Recurrent Aphthous Stomatitis. *Drug Des. Dev. Ther.* **2021**, *15*, 4071−4089.

(3) Kamiya, K.; Takeuchi, S. Giant Liposome Formation toward the Synthesis of Well-Defined Artificial Cells. *J. Mater. Chem. B* **2017**, *5*, 5911−5923.

(4) Llopis-Lorente, A.; Schotman, M. J. G.; Humeniuk, H. V.; van Hest, J. C. M.; Dankers, P. Y. W.; Abdelmohsen, L. K. E. A. Artificial Cells with Viscoadaptive Behavior Based on Hydrogel-Loaded Giant Unilamellar Vesicles. *Chem. Sci.* **2024**, *15*, 629−638.

(5) Barba-Bon, A.; Pan, Y.-C.; Biedermann, F.; Guo, D.-S.; Nau, W. M.; Hennig, A. Fluorescence Monitoring of Peptide Transport Pathways into Large and Giant Vesicles by Supramolecular Host-Dye Reporter Pairs. *J. Am. Chem. Soc.* **2019**, *141*, 20137−20145.

(6) Sakaino, H.; Sawayama, J.; Kabashima, S.-i.; Yoshikawa, I.; Araki, K. Dry Micromanipulation of Supramolecular Giant Vesicles on a Silicon Substrate: Highly Stable Hydrogen-Bond-Directed Nanosheet Membrane. *J. Am. Chem. Soc.* **2012**, *134*, 15684−15687.

(7) Ayala, Y. A.; Omidvar, R.; Römer, W.; Rohrbach, A. Thermal Fluctuations of the Lipid Membrane Determine Particle Uptake into Giant Unilamellar Vesicles. *Nat. Commun.* **2023**, *14*, 65.

(8) Kindt, J. T.; Szostak, J. W.; Wang, A. N. Bulk Self-Assembly of Giant, Unilamellar Vesicles. *ACS Nano* **2020**, *14*, 14627−14634.

(9) Tsumoto, K.; Matsuo, H.; Tomita, M.; Yoshimura, T. Efficient Formation of Giant Liposomes through the Gentle Hydration of Phosphatidylcholine Films Doped with Sugar. *Colloids Surf., B* **2009**, *68*, 98−105.

(10) Li, Q. C.; Wang, X. J.; Ma, S. H.; Zhang, Y.; Han, X. J. Electroformation of Giant Unilamellar Vesicles in Saline Solution. *Colloids Surf., B* **2016**, *147*, 368−375.

(11) Micheletto, Y. M. S.; Marques, C. M.; Silveira, N. P. d.; Schroder, A. P. Electroformation of Giant Unilamellar Vesicles: Investigating Vesicle Fusion Versus Bulge Merging. *Langmuir* **2016**, *32*, 8123−8130.

(12) Shimanouchi, T.; Umakoshi, H.; Kuboi, R. Kinetic Study on Giant Vesicle Formation with Electroformation Method. *Langmuir* **2009**, *25*, 4835−4840.

(13) Kuribayashi, K.; Tresset, G.; Coquet, P.; Fujita, H.; Takeuchi, S. Ieee In Electroformation of Giant Liposomes in Microfluidic Channels. *13th International Conference on Solid-State Sensors, Actuators and Microsystems, Seoul, South Korea, June 05-09*: Seoul, South Korea, 2006; Vol. *17*, pp 3121−3126.

(14) Georgieva, R.; Koumanov, K.; Momchilova, A.; Tessier, C.; Staneva, G. Effect of Sphingosine on Domain Morphology in Giant Vesicles. *J. Colloid Interface Sci.* **2010**, *350*, 502−510.

(15) Rems, L.; Usaj, M.; Kanduser, M.; Rebersek, M.; Miklavcic, D.; Pucihar, G. Cell Electrofusion Using Nanosecond Electric Pulses. *Sci. Rep.* **2013**, *3*, 3382.

(16) Tamba, Y.; Terashima, H.; Yamazaki, M. A Membrane Filtering Method for the Purification of Giant Unilamellar Vesicles. *Chem. Phys. Lipids* **2011**, *164*, 351−358.

(17) Jing, H. Y.; Sinha, S.; Sachar, H. S.; Das, S. Interactions of Gold and Silica Nanoparticles with Plasma Membranes Get Distinguished by the Van Der Waals Forces: Implications for Drug Delivery, Imaging, and Theranostics. *Colloids Surf., B* **2019**, *177*, 433−439.

(18) Fragasso, A.; De Franceschi, N.; Stömmer, P.; van der Sluis, E. O.; Dietz, H.; Dekker, C. Reconstitution of Ultrawide DNA Origami Pores in Liposomes for Transmembrane Transport of Macromolecules. *ACS Nano* **2021**, *15*, 12768−12779.

(19) Enkavi, G.; Javanainen, M.; Kulig, W.; Róg, T.; Vattulainen, I. Multiscale Simulations of Biological Membranes: The Challenge to Understand Biological Phenomena in a Living Substance. *Chem. Rev.* **2019**, *119*, 5607−5774.

(20) Gutierrez, M. G.; Mansfield, K. S.; Malmstadt, N. The Functional Activity of the Human Serotonin 5-HT 1A Receptor Is Controlled by Lipid Bilayer Composition. *Biophys. J.* **2016**, *110*, 2486−2495.

(21) Sankhagowit, S.; Wu, S. H.; Biswas, R.; Riche, C. T.; Povinelli, M. L.; Malmstadt, N. Corrigendum to "The dynamics of giant unilamellar vesicle oxidation probed by morphological transitions" [Biochim. Biophys. Acta 1838 (2014) 2615−2624]. *Biochim. Biophys. Acta, Biomembr.* **2015**, *1848*, 433.

(22) Nishimura, K.; Suzuki, H.; Toyota, T.; Yomo, T. Size Control of Giant Unilamellar Vesicles Prepared from Inverted Emulsion Droplets. *J. Colloid Interface Sci.* **2012**, *376*, 119−125.

(23) Howse, J. R.; Jones, R. A. L.; Battaglia, G.; Ducker, R. E.; Leggett, G. J.; Ryan, A. J. Templated Formation of Giant Polymer Vesicles with Controlled Size Distributions. *Nat. Mater.* **2009**, *8*, 507−511.

(24) Taylor, P.; Xu, C.; Fletcher, P. D. I.; Paunov, V. N. Fabrication of 2d Arrays of Giant Liposomes on Solid Substrates by Microcontact Printing. *Phys. Chem. Chem. Phys.* **2003**, *5*, 4918−4922.

(25) Gertrude Gutierrez, M.; Yoshida, S.; Malmstadt, N.; Takeuchi, S. Photolithographic Patterned Surface Forms Size-Controlled Lipid Vesicles. *APL Bioeng.* **2018**, *2*, 016104.

(26) Fan, T.; Wang, Q.; Hu, N.; Liao, Y. J.; Chen, X.; Wang, Z. Y.; Yang, Z.; Yang, J.; Qian, S. Z. Preparation of Giant Lipid Vesicles with Controllable Sizes by a Modified Hydrophilic Polydimethylsiloxane Microarray Chip. *J. Colloid Interface Sci.* **2019**, *536*, 53−61.

(27) Kang, D. H.; Han, W. B.; Choi, N.; Kim, Y. J.; Kim, T. S. Tightly Sealed 3d Lipid Structure Monolithically Generated on Transparent Su-8 Microwell Arrays for Biosensor Applications. *ACS Appl. Mater. Interfaces* **2018**, *10*, 40401−40410.

(28) Le Berre, M.; Yamada, A.; Reck, L.; Chen, Y.; Baigl, D. Electroformation of Giant Phospholipid Vesicles on a Silicon Substrate: Advantages of Controllable Surface Properties. *Langmuir* **2008**, *24*, 2643−2649.

(29) Wang, Q.; Li, W. M.; Hu, N.; Chen, X.; Fan, T.; Wang, Z. Y.; Yang, Z.; Cheney, M. A.; Y ang, J. Ion concentration effect (Na+ and Cl−) on lipid vesicle formation. *Colloids Surf., B* **2017**, *155*, 287−293.

(30) Weinberger, A.; Tsai, F. C.; Koenderink, G. H.; Schmidt, T. F.; Itri, R.; Meier, W.; Schmatko, T.; Schröder, A.; Marques, C. Gel-Assisted Formation of Giant Unilamellar Vesicles. *Biophys. J.* **2013**, *105*, 154−164.

(31) Horger, K. S.; Estes, D. J.; Capone, R.; Mayer, M. Films of Agarose Enable Rapid Formation of Giant Liposomes in Solutions of Physiologic Ionic Strength. *J. Am. Chem. Soc.* **2009**, *131*, 1810−1819.

(32) Pazzi, J.; Subramaniam, A. B. Nanoscale Curvature Promotes High Yield Spontaneous Formation of Cell-Mimetic Giant Vesicles on Nanocellulose Paper. *ACS Appl. Mater. Interfaces* **2020**, *12*, 56549−56561.

(33) Papahadjopoulos, D.; Nir, S.; Düzgünes, N. Molecular Mechanisms of Calcium-Induced Membrane Fusion. *J. Bioenerg. Biomembr.* **1990**, *22*, 157−179.

(34) Ohki, S.; Arnold, K. Surface Dielectric Constant, Surface Hydrophobicity and Membrane Fusion. *J. Membr. Biol.* **1990**, *114*, 195−203.

(35) Sugahara, K.; Morimoto, Y.; Takamori, S.; Takeuchi, S. A Dynamic Microarray Device for Pairing and Electrofusion of Giant Unilamellar Vesicles. *Sens. Actuators, B* **2020**, *311*, 127922.

(36) Weingaertner, A.; Kemmer, G.; Mueller, F. D.; Zampieri, R. A.; dos Santos, M. G.; Schiller, J.; Pomorski, T. G. Leishmania Promastigotes Lack Phosphatidylserine but Bind Annexin V Upon Permeabilization or Miltefosine Treatment. *PLoS One* **2012**, *7*, No. e42070.

(37) Peruzzi, J.; Gutierrez, M. G. L.; Mansfield, K.; Malmstadt, N. Dynamics of Hydrogel-Assisted Giant Unilamellar Vesicle Formation from Unsaturated Lipid Systems. *Langmuir* **2016**, *32*, 12702−12709.

(38) Mertins, O.; da Silveira, N. P.; Pohlmann, A. R.; Schröder, A. P.; Marques, C. M. Electroformation of Giant Vesicles from an Inverse Phase Precursor. *Biophys. J.* **2009**, *96*, 2719−2726.

(39) Oropeza-Guzman, E.; Rios-Ramirez, M.; Ruiz-Suarez, J. C. Leveraging the Coffee Ring Effect for a Defect-Free Electroformation of Giant Unilamellar Vesicles. *Langmuir* **2019**, *35*, 16528−16535.

https://doi.org/10.1021/acsami.4c07934
ACS Appl. Mater. Interfaces 2024, 16, 45948−45955